ELSEVIER

Journal of Structural Geology 29 (2007) 530–540

JOURNAL OF STRUCTURAL GEOLOGY

www.elsevier.com/locate/jsg

Hypoplastic simulation of normal faults without and with clay smears

G. Gudehus [a,*], C. Karcher [b]

[a] *Institute of Soil and Rock Mechanics, Engler-Bunte-Ring 14, 76131 Karlsruhe, Germany*
[b] *RWE Power AG, Stüttgenweg 2, 50935 Köln, Germany*

Received 9 August 2004; received in revised form 19 July 2006; accepted 28 September 2006
Available online 29 November 2006

Abstract

The main objective of the present paper is to simulate the tectonic evolution of normal faults by means of hypoplasticity. This constitutive concept is introduced with state limits for sand-like and clay-like materials. Combined with conservation laws, and initial and boundary conditions, hypoplastic relations provide normal fault patterns, which are validated by model tests. For a cross section of the Lower Rhenish Basin with synsedimentary subsidence, the observed normal fault pattern is essentially reproduced. A realistic evolution of a single normal fault with the distortion of a clay layer into a clay smear is also obtained. The potential of our method for other tectonic simulations is indicated.

Animations of calculated evolutions are available in the Internet via http://www.ibf.uni-karlsruhe.de/material.html.

Keywords: Normal faults; Clay smears; Numerical simulation; Hypoplasticity

1. Introduction

There are striking similarities of soil deformations in a model box and tectonic deformations in the earth crust. This led to definitions of fault and shear systems, which are widely recognized in structural geology. Limit state plasticity concepts of soil mechanics are used for estimating stress fields from observed fault patterns (Mandl, 1988). This approach leaves open a number of questions:

- what is the influence of pressure and density,
- what is the role of time and viscosity,
- why do shear band patterns arise, and
- what kind of simulations can substitute model tests?

A key issue is the constitutive relations describing the mechanical behaviour of formation materials. Critical State Soil Mechanics (CSSM, Schoefield and Wroth, 1968) goes beyond conventional limit state plasticity. For critical states with stationary shearing, a pressure independent ratio of deviatoric and mean stress is proposed with a friction angle φ_c, and a void ratio e_c that decreases linearly with the logarithm of effective pressure p'. For isotropic first compression, a higher void ratio e_i depends likewise on p'. For higher than critical stress ratios, dilated shearing and the same decrease of e with higher p' is proposed. A lower bound void ratio was later proposed by Schoefield (2001) and related with tensile cracking. Various elastoplastic relations based on CSSM are used in geotechnical engineering.

Taking over CSSM for simulation of tectonic deformations would reveal some shortcomings: the linear e-log p' dependence can fail for big p', the lower e-bound can only be reached by decompression, and viscous effects are not allowed for. *Hypoplastic* relations imply state limits as asymptotic solutions (Gudehus, 1996), and were extended by polar terms for shear localizations (Tejchman and Gudehus, 2001). Such sand-like materials are introduced in Section 2. Clays are markedly rate-dependent as their particles are squashy, so they reveal creep and relaxation. Visco-plastic relations on the base of CSSM have been proposed for them (Adachi and Oka, 1982), but have as yet been scarcely used. Visco-hypoplastic relations (Niemunius, 2003) have a wider range of application. They represent clay-like materials and are introduced in Section 3.

* Corresponding author. Tel.: +49 7216 082220; fax: +49 7216 96096.
E-mail address: gerd.gudehus@ibf.uni-karlsruhe.de (G. Gudehus).

0191-8141/$ - see front matter © 2006 Elsevier Ltd. All rights reserved.
doi:10.1016/j.jsg.2006.09.011

Normal faulting can be considered as a touchstone for the use of hypoplasticity for tectonic deformations. This is first shown in Section 4 for initially homogeneous formations. Swarms of normal shear bands have been observed in model sand boxes, e.g. Wolf et al. (2003). We obtain such realistic shear band patterns that they can substitute model tests and provide more insight. For field-size problems finite element mesh sizes down to a few grain diameters are neither feasible nor necessary. For a known case of synsedimentary subsidence, realistic swarms of normal and antithetic faults are obtained.

A mechanism for the evolution of *clay smears* in normal faults was proposed by Lehner and Pilaar (1995). They postulate a viscous extrusion by a pressure gradient from the far-field towards the fault. As shown in Section 5, we obtain a combination of extrusion and shearing and a pressure gradient towards the fault. Furthermore, we obtain an asymptic clay smear thickness and a continued widening of the fault, and increasing swarms of antithetic shears. This is validated by observations (Weber et al., 1978).

Conclusions and an outlook are given in Section 6. It appears that the questions raised at the onset of this Introduction can be answered more and more by means of hypoplastic simulations. Tectonic deformations more complex than normal faulting could also be grasped.

2. Hypoplastic behaviour of psammoids

A *psammoid* (Greek psammos = sand) is an idealized substitute of a granular soil—like silt, sand or gravel. Granular permanence is assumed, i.e. changes of grains except for plastic flats at their contacts are neglected. Three limit void ratios depend on the mean solid partial pressure p_s as shown in Fig. 1a. The upper bound e_i denotes e for an isotropic compression starting from a very loose state, e_c is the critical void ratio for stationary shearing, and e_d denotes a lower bound approached by cyclic shearing with constant p_s and small strain amplitudes.

The curves of Fig. 1a are described (Bauer, 1996) by

$$\frac{e_i}{e_{io}} = \frac{e_c}{e_{co}} = \frac{e_d}{e_{do}} = \exp\left[-\left(\frac{3p_s}{h_c}\right)^n\right]. \tag{1}$$

The granular hardness h_s ranges from ca. 10 MPa to 10 GPa, and the exponent n from ca. 0.3 to 0.6. The prefactors e_{io}, e_{co} and e_{do} have nearly constant ratios, $e_{io}/e_{co} \approx 1.1$ and $e_{do}/e_{co} \approx 0.6$, so only e_{co} is needed. A relative void ratio

$$r_e = (e - e_c)/(e - e_d), \tag{2}$$

is defined by the actual e and the p_s-dependent limit values e_c and e_d.

The stress state of the grain skeleton is described by a tensor. With cylindrical symmetry, like in a triaxial apparatus, axial and radial components σ_{s1} and $\sigma_{s2} = \sigma_{s3}$ can be represented in a plane (Fig. 1b), and substituted by $p_s = (\sigma_{s1} + 2\sigma_{s2})/3$ and a deviatoric angle $\psi_\sigma = \operatorname{atan}\sqrt{2}(\sigma_{s1} - \sigma_{s2})/3p_s$. Hypoplastic relations express skeleton stress rates as functions of stress, void ratio and strain rate, viz.

$$\dot{\sigma}_{si} = f_s\left(L_{ij}\varepsilon_j + r_e^\alpha N_i D\right), \tag{3}$$

with summation in j and $i = 1,2$ for cylindrical symmetry. $\dot{\varepsilon}_1$ and $\dot{\varepsilon}_2 = \dot{\varepsilon}_3$ can be substituted by the rate of volume change $\dot{\varepsilon}_v = \dot{\varepsilon}_1 + 2\dot{\varepsilon}_2$, and a direction angle $\psi_\varepsilon = \operatorname{atan}\sqrt{2}(\dot{\varepsilon}_1 - \dot{\varepsilon}_2)/\dot{\varepsilon}_v$, Fig. 1c. $D = \sqrt{\dot{\varepsilon}_1^2 + 2\dot{\varepsilon}_2^2}$ denotes the modulus of strain rate. L_{ij} and N_i are functions of ψ_σ and the critical friction angle φ_c. f_s is determined by Eq. (1) and therefore proportional to h_s and $(\rho_s/h_s)^{1-n}$. For state limits, simple relations hold between $\psi_{\dot{\varepsilon}}$, ψ_σ and r_e, Fig. 1d and e. For an isotropic compression from $e = e_{io'}$ (i), $\psi_\sigma = \psi_{\dot{\varepsilon}} = 0$ holds with $r_e = (e_{io} - e_{co})/(e_{co} - e_{do})$. For stationary shearing at critical states, i.e. $\psi_{\dot{\varepsilon}} = \pm 90^\circ$ and $\dot{\sigma}_{si} = 0$ the stress condition reads

$$(\sigma_{s1} - \sigma_{s2})^2/(\sigma_{s1} + \sigma_{s2})^2 = \sin^2\varphi_c. \tag{4}$$

This means two different ψ_σ for axial shortening and stretching (c and −c). $e = e_c$ means $r_e = 1$. Axial splitting with $\sigma_{s2} \to 0$ and $\dot{\varepsilon}_1 \to 0$ and discing with $\sigma_{s1} = 0$ and $\dot{\varepsilon}_2 \to 0$ are unattainable extreme cases with $r_e = 0$ (d and −d). For peak states in between critical states and splitting Eq. (4) holds with a peak friction angle φ_p instead of φ_c and with dilation.

State limits are asymptotic solutions of Eq. (3) for a given $\psi_{\dot{\varepsilon}}$ and can therefore be called *attractors* (whereas they are assumed *a priori* in elastoplastic relations). This concept works also for other than cylindrically symmetric deformations, in particular simple shearing, and has been validated (Gudehus, 2006). It implies *shear localization* for peak states in two conjugate planes inclined by ca. $45^\circ - \varphi_p/2$ against the σ_{s1}-axis for cylindrical shortening. Splitting or discing may be interpreted as anomalous shear localization with $\varphi_p = 90^\circ$.

Evolutions of state and shape of representative volume elements (RVE) can be simulated numerically with the hypoplastic relation (3). An initial state has to be assumed within the allowed range of stresses and void ratios. Two of the four components σ_{s1}, σ_{s2}, ε_1 and ε_2 can be given as time-dependent boundary conditions, and two can be calculated using Eq. (3). Other than with elastoplastic relations, strength and stiffness are thus derived and not assumed *a priori*.

Shear bands arise throughout an RVE beyond a peak state so that it is no more homogeneous. This can be modelled by hypoplasticity with finite elements and different sophistications, e.g. for stretching of a strip between two smooth plates with constant lateral pressure (Fig. 2a). A zig-zag pattern with reflections at the plates is obtained by means of Eq. (3) if $e < e_c$ holds at the onset. e tends to e_c in the bands; in the end, the whole strip attains a critical state. One can approximate the overall behaviour using Eq. (4) with a peak friction angle φ_p instead of φ_c and with spatial averages $\overline{\sigma}_{s1}, \overline{\sigma}_{s2}$ and $\overline{e}$ of the state variables.

These findings are partly mesh dependent. Peak stress ratios and shear band inclinations can be obtained realistically if the mesh is not too coarse. However, the width of primary shear bands is determined by the element size, and more so the subsequent evolution. This lack of objectivity can be overcome by polar quantities (Gudehus and Nübel, 2004). The shear band width is restricted to ca. 5–15 grain diameters by the

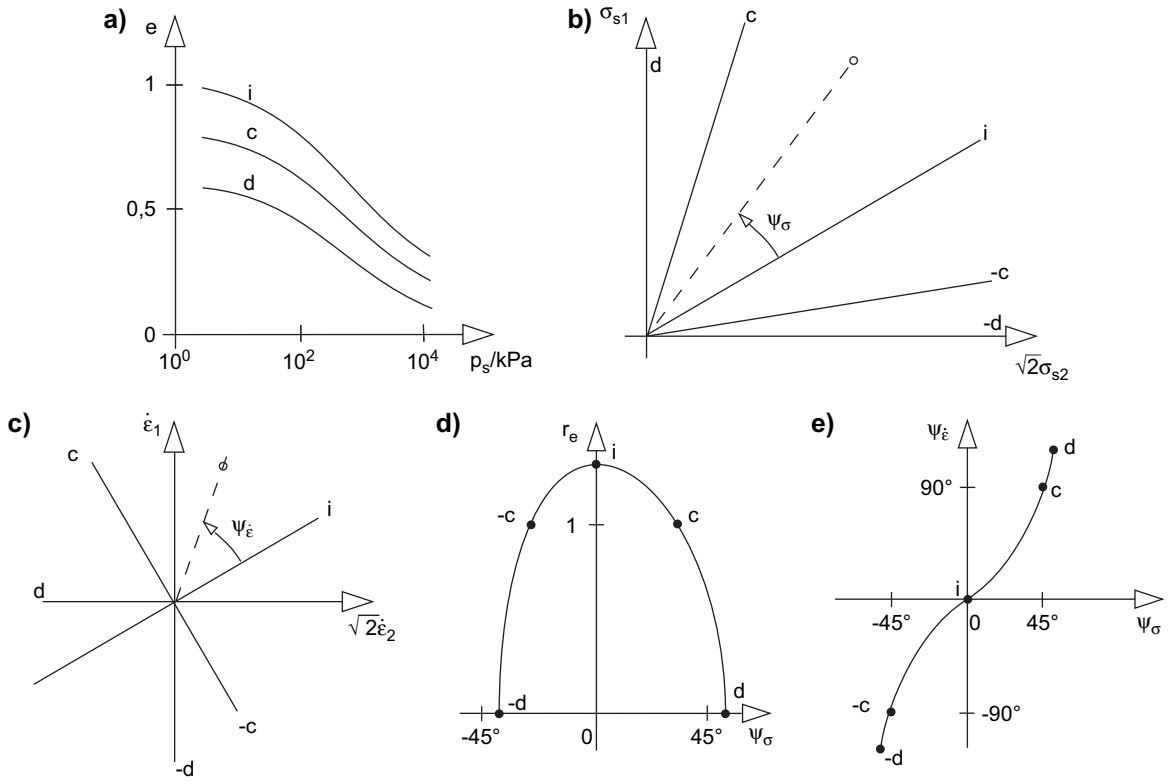

Fig. 1. State limits of a psammoid: (a) void ratio vs. skeleton pressure, (b) skeleton stress plane, (c) strain rates, (d) relative void ratio vs. stress direction, and (e) strain rate direction vs. stress direction.

resistance to strong relative rotations. With this extension the calculated evolution of patterns, e.g. Fig. 2b, is more realistic (cf. Desrues, 1998). In between the size of ca. 10 grains and the height of the strip the pattern has no preferred scale, it is fractal. This justifies the neglection of polar quantities if the finite elements are far bigger than the grains and far smaller than the strip height such as in Fig. 2a. This may be sufficient for modelling tectonic changes of state and shape, but details of shear bands are thus not grasped.

3. Visco-hypoplastic behaviour of peloids

Peloids (Greek pelos = clay) have finer, softer and more angular particles than psammoids. As shown in Fig. 3a, their

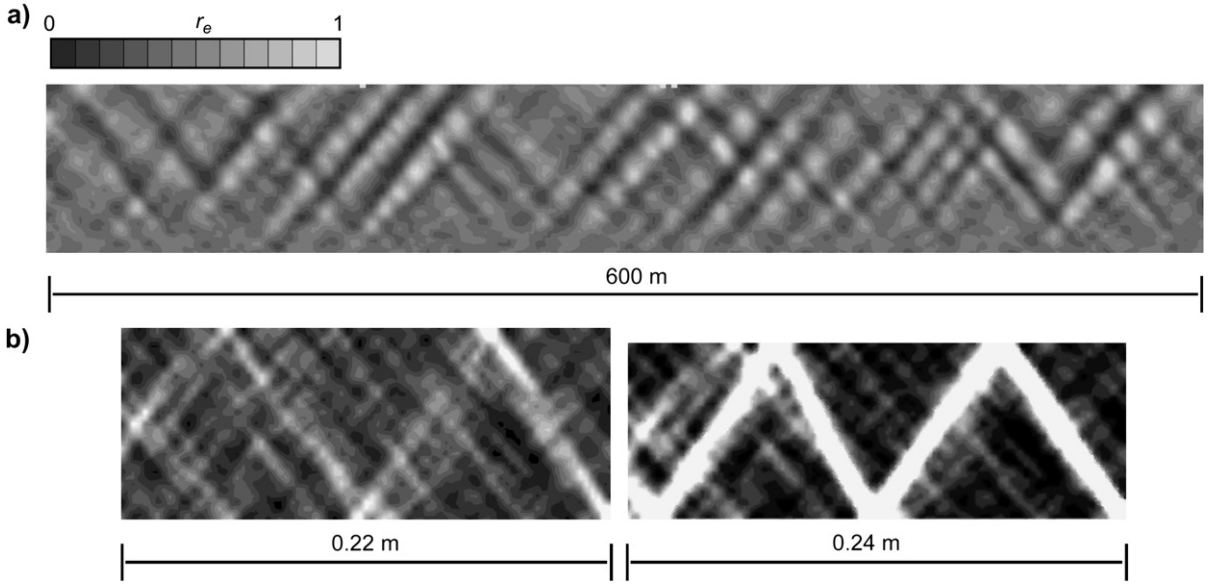

Fig. 2. Shear bands in a stretched psammoid rectangle, calculated without (a) and with polar terms (b).

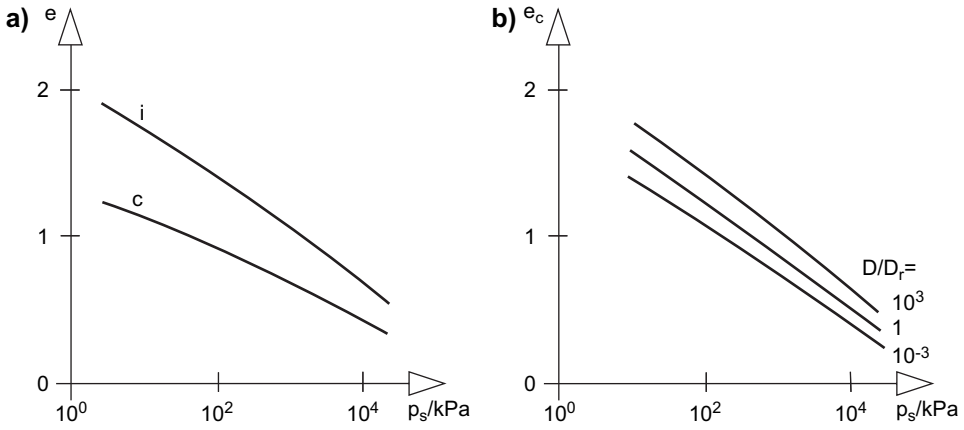

Fig. 3. (a) Limit void ratios of a peloid vs. pressure for constant strain rates D, and (b) critical void ratios for different strain rates.

limit void ratios for isotropic compression (i) and stationary shearing (c) are higher therefore than for psammoids with low pressure p_s, and lower for high p_s. Niemunius (2003) uses the approximation

$$\ln\left(\frac{1+e_r}{1+e}\right) = \lambda \ln(p_s/p_r), \tag{5}$$

with a compression index λ and reference values p_r and $e = e_r$ for $p_s = p_r$. Other than by Eq. (1) p_r is not objective, Eq. (5) fails for $p_s \to 0$ and $p_s \to \infty$, and a lower bound e_d is not specified. Nevertheless Eqs. (5) and (1) can agree fairly well in the working range with $h_s = p_r/2.7$ and $\lambda = e_{cr}n$.

As shown in Fig. 3b, for stationary shearing the limit void ratios are *argotropic*, i.e. velocity-dependent. This is due to thermally activated dislocations in solid particles. This can be captured by means of the argotropic reference pressure

$$p_r = p_{rr}(D/D_r)^{I_v}, \tag{6}$$

with the stretching rate D, a reference rate D_r, a reference pressure p_{rr} for $D = D_r$ and the viscosity index I_v which ranges from ca. 0.02 to 0.05 for lowly to highly plastic clays. The stress ratio at critical states is given by Eq. (4) with a rate-independent critical friction angle φ_c ranging from ca. 10° to 30° for highly to lowly plastic clays. Combining Eq. (4) with Eq. (5) and (b) for a given e leads to

$$\sigma_1 - \sigma_2 = \frac{6\sin\varphi_c}{3-\sin\varphi_c} p_e (D/D_r)^{I_v} \tag{7}$$

with an e-equivalent pressure p_e by inversion of Eq. (5), with p_{rr} instead of p_e (Eq. (7)), Eq. (7) agrees with Norton's creep law for solids. The dependence of stress obliquity ψ_σ on ψ_ε for state limits as plotted in Fig. 1e is taken over to peloids. The equivalent pressure equals the mean one, $p_e = p_s$, for state limits with $D = D_r$.

As with water-saturated psammoids, the total pressure p of a peloid is related with pore water pressure p_w and mean skeleton pressure p_s by

$$p = p_s + p_w, \tag{8}$$

and only p_s is related with deformations of the skeleton. This holds true as mineral particles are neutral with respect to p_w. If volume changes are very slow p_w is determined by hydraulic boundary conditions.

The *visco-hypoplastic* relations of Niemunius (2003) can be written as

$$\dot\sigma_{si} = f_s\left[L_{ij}\dot e_j - \left(\frac{p_s}{p_e}\right)^{1/I_v} N_i D_r\right], \tag{9}$$

with $i = 1,2$ for cylindrical symmetry and summation for $j = 1,2$. L_{ij} and N_i are the same functions of ψ_σ and φ_c, and f_s is the same function of p_s, as for psammoids by Eq. (3). $p_e = p_s$ holds for state limits with $D = D_r$, the same dependence of p_e on e and ψ_σ is used also for other states. State limits are again obtained as asymptotic solutions or *attractors* for given strain rates. *Creep* is obtained from Eq. (9) for constant skeleton stress, i.e. $\dot\sigma_{si} = 0$. It is contractant and slowing down (often called primary) for lower than critical, stationary (secondary) for critical $|\psi_\sigma|$ and accelerating with dilation (tertiary) for more than critical $|\psi_\sigma|$. *Relaxation* is obtained by Eq. (9) for $\dot\varepsilon_i = 0$.

Shear localization can be obtained principally as with psammoids, but pore water and viscosity of the solid play a bigger role. The low permeability prevents seepage and causes changes of p_w for rapid shearing with constant p even if it is localized to narrow bands. Splitting with zero skeleton pressure normal to cracks may again be considered as an anomalous extreme case with $\varphi_p \to 90°$. It requires more rapid shearing for lower densities, and big enough negative p_w for cavitation. Thus, the interaction of solid particle skeleton and pore water requires a sophisticated analysis for rapid tectonic deformations. In this paper, we consider only slow deformations so that p_w may be assumed as hydrostatic. As with psammoids, details of shear band patterns could be obtained with additional polar quantities. In the sequel we consider spatial averages of finite element meshes, which are by several orders of magnitude wider than a few solid particles.

4. Simulated normal faults in homogeneous formations

Stretching of a small dry psammoid strip with free surface was simulated with polar quantities (Gudehus and Nübel, 2004), Fig. 4. The element size is about two grain diameters, so details of shear bands can be modelled. A layer height of 50 and length of 200 elements render possible a good resolution. The average initial relative void ratio was lower than critical, $0 < \overline{r}_e < 1$. A realistic spatial fluctuation of r_e was generated by means of random numbers. An initial stress field was generated by stepwise increase of gravity from 0 to g. The average components are proportional to depth z,

$$\overline{\sigma}_{s1} = \rho g z, \quad \overline{\sigma}_{s2} = K_0 \sigma_{s1}, \tag{10}$$

with $\rho = \rho_s e/(1+e)$ from solid density ρ_s, and $K_0 \approx 1 - \sin\varphi_c$. The calculated initial spatial fluctuation of skeleton stress is negligible.

A minute pressure p_s in the uppermost nodal points prevents numerical problems with $p_s = 0$. The left wall is fixed and perfectly smooth, it serves as a symmetry line. The base is stretched uniformly, the right wall is perfectly smooth and moves with the base. With 10% stretching a zig-zag pattern of shear bands is achieved, it is visualised by strips of increased r_e, Fig. 4a. With 20% stretching (b) a critical state with $r_e = 1$ is reached in the primary shear bands, and secondary bands arise between them. Graben-like offsets at the free surface follow the primary shear bands.

The average of the relative void ratio increases with stretching, and also its spatial fluctuation. This confirms the assumption that the initial fluctuation is bigger for a higher initial average $\overline{r}_e$. The spatial fluctuation of the horizontal pressure increases with stretching, whereas it remains negligible for the vertical pressures. The average shear band inclination and stress ratio are

$$\overline{\Theta}_a \approx 45^\circ + \varphi_p/2, \quad \overline{\sigma}_{s2}/\overline{\sigma}_{s2} \approx \tan^2\left(45^\circ - \varphi_p/2\right), \tag{11}$$

with a peak friction angle φ_p depending on r_e. Numerical problems prevented a simulation beyond 20% stretching. It appears that the strip tends to an overall critical state with fluctuations over lengths from a few grains to the layer height. These findings do not depend on the element width if this is nearly as small as the grain size.

Similar observations were made in model tests. With other boundary conditions the agreement of calculated and observed shear band patterns is even better (Gudehus and Nübel, 2004). This means than one may substitute tectonic sandbox experiments by hypoplastic simulations, and can get more insight. This holds true at least for plane strain; for three-dimensional deformations, the computer capacity is still a limiting factor.

For a field-size layer with similar initial and boundary conditions, Fig. 5, the mesh size must be bigger by orders of magnitude than the grain size. The psammoid may be water saturated with hydrostatic pore water pressure. A pattern of shear bands arises with ca. 10% stretching; in the bands critical states are nearly reached (a). With ca. 20% stretching the pattern gets more marked, and graben-like offsets at the free surface indicate the outcrops of primary shear bands (b). The average stress ratio can be estimated by Eq. (11b), but the inclination is lower than by Eq. (11a) for a big stretching.

Shear band thickness and spatial resolution are given by the mesh size. The fluctuations increase with stretching qualitatively, as in Fig. 4 with a finer resolution fluctuations with smaller wavelengths would be produced. For an objective lower cut-off the finest meshes should be calculated with polar quantities. The upper bound of fluctuation wavelengths is the layer thickness. This is similar as with the strip squeezed between two smooth plates, Fig. 2. With continued stretching the layer tends to an overall critical state and rather fractal fluctuations.

Fig. 5 suggests that tectonic deformations can also be simulated with other boundary conditions if a resolution down to a few grains is not intended. This holds true also for peloids with nearly constant stretching rates if these are low enough so that pore water pressures remain nearly hydrostatic (cf. Section 3). For a first approximation a composite of psammoids and peloids could be substituted by a homogeneous body with average hypoplastic parameters. The boundary conditions could be more realistic than for Fig. 5, but they remain partly fictitious. They can be justified by comparison of calculated and observed fault patterns. This is a kind of validation if the formation materials reveal rather hypoplastic behaviour, provided that the calculated pattern is robust with respect to indiscernible details of boundary conditions.

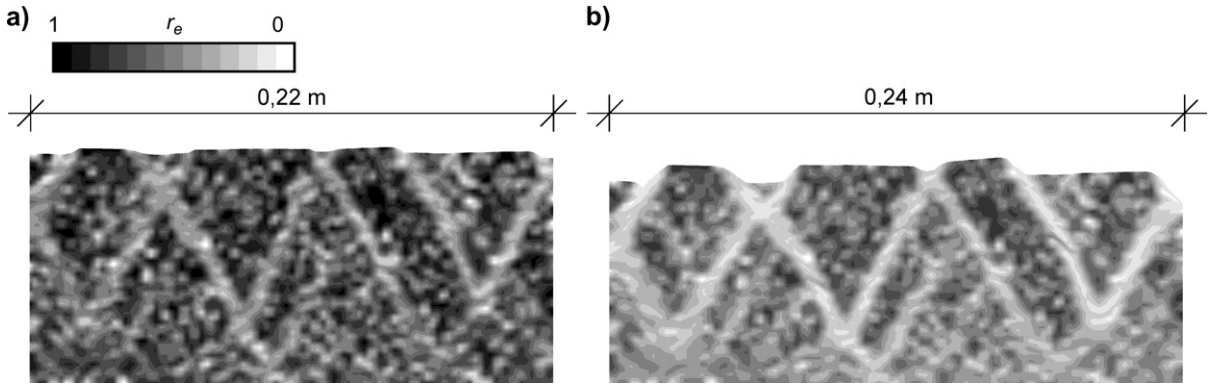

Fig. 4. Shear bands of a small psammoid layer for ca. 10% (a) and 20% (b) stretching, calculated with polar terms.

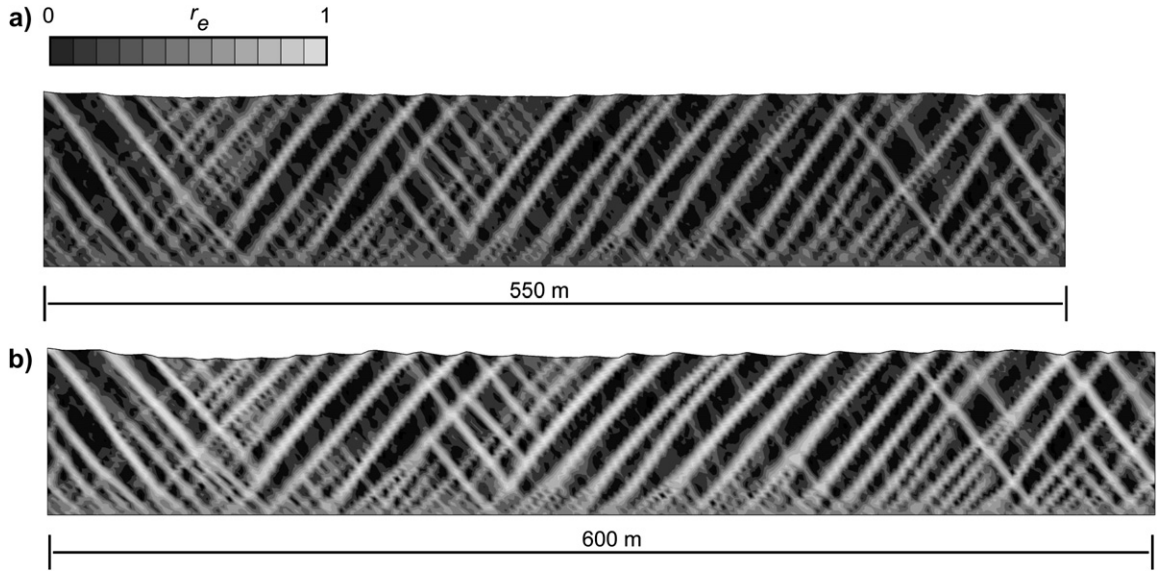

Fig. 5. Shear bands of a field-size psammoid layer with 10% (a) and 20% stretching (b), calculated without polar terms.

Synsedimentary subsidence and *stretching* may serve as an example (Karcher, 2003). Cross section and average parameters are adapted to the Lower Rhenish Basin West of Cologne (Knufinke and Kothen, 1995). Initial and boundary conditions are assumed as shown in Fig. 6a and b. Right of a symmetry line, a weightless hill upon a horizontal layer with gravity and $r_e \approx 0.2$ (dense) constitutes the initial state. Alongside with an increasing subsidence of the base towards the middle, and thus with stretching right of its turning point, the weight of the hill is increased up to the real amount. The latter

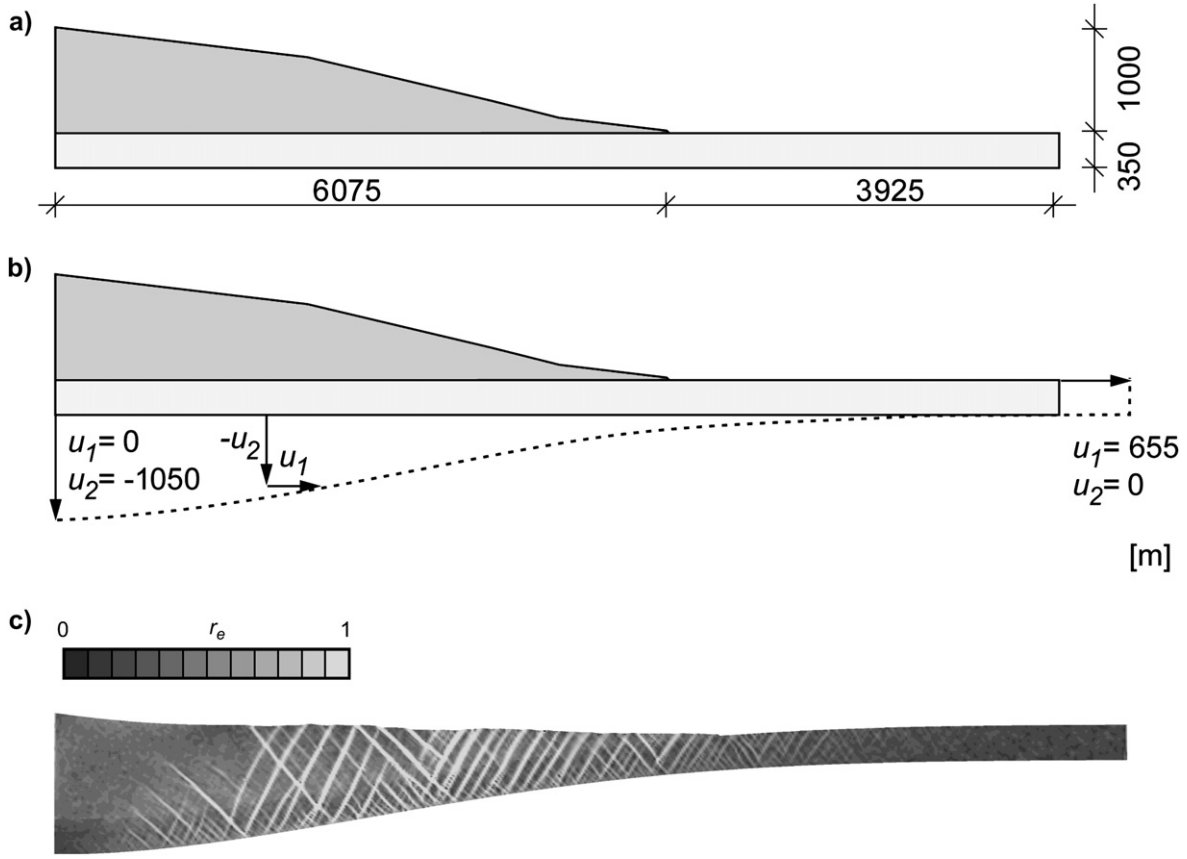

Fig. 6. Simulated synsedimentary faulting; initial (a) and final (b) configuration, and (c) pattern of shear zones.

corresponds to syntectonic sedimentation, and leads to an r_e, which is somewhat reduced by compressive creep within 2×10^7 years.

The calculated fault pattern is shown in Fig. 6c by intensities of dilation. A swarm of normal faults can be seen in the range of maximal base stretching. They dip towards the middle with an average angle by Eq. (11a), and less towards the base. Less marked swarms of antithetic faults appear left and right of the normal ones. The distance of the latter is about 1/4 of the original layer thickness, this can also be seen from steps at the outcrops. In the shear bands, the material is dilated up to critical states, and their thickness equals the mesh size.

The calculated pattern has a lot in common with the one documented by Knufinke and Kothen (1995), Fig. 7. Normal faults right of the deepest subsidence dip towards the same. The reported dip angles are slightly lower than the calculated ones, and lower near the base. Minor swarms of antithetic faults have also been found. The distance of main faults is bigger than 1/4 of the sediment thickness, but faults are also in the rock base. Left of the deepest subsidence the main dip is not symmetric as assumed in our simulation. The rather good agreement could only be achieved with the boundary conditions of Fig. 6a and b. It appears that a better agreement cannot be achieved with the assumed homogeneity and symmetry.

5. Simulated evolution of a clay smear

Consider a section of two psammoid layers with a thinner peloid layer in between, which is subjected to normal faulting, Fig. 8. Initially (a) the shape may be undistorted, the skeleton stress may be given by gravity and the ratio $\sigma_{sh}/\sigma_{sv} \approx 1 - \sin \varphi_c$. The relative void ratios may be $r_e \approx$ and …, the pore water may exist and continue to do so in a hydrostatic state. The base may be dislocated without dilation, left and right smooth walls follow this relative displacement, and the top skeleton pressure is assumed to remain unchanged.

These boundary conditions represent an imposed normal faulting. The clay seam in the middle is so thin as against the total height and width that its evolution is mainly determined by far-field pressure and dislocation, and not by more details of far-field boundary conditions. Further steps of the calculated evolution of shape indicate a widening fault and a thinning clay smear, Fig. 8b–d. Crosses for principal skeleton stress reveal a reduction of pressure towards the clay smear, and a deviation of the σ_{s1}-direction from the vertical as in the far-field, so that it makes ca. 45° with the fault.

The obtained changes of fault width d_f and clay smear thickness d_c with offset s referred to the initial clay layer height h_c are plotted in Fig. 9. For large s/h_c, the calculated d_f/h_s increases almost linearly with s/h_c (a), whereas d_c/h_c attains an asymptote (b). The peloid in the clay smear is slightly dilated to a critical state of stationary shearing, and the neighbouring psammoid reaches such states in the shear bands. The principal stress direction makes an angle of ca. 45° with the shearing direction.

The mechanism for large deformations may be simplified as follows. With a further offset in the direction of the normal fault this is widened. A corresponding part of the source clay layer enters the fault, whereas the central part of the clay smear experiences stationary shearing. Dilation towards the critical state has a minor influence on the kinematics. More precisely speaking, the shearing is localized in rather fractal swarms of normal and antithetic shear bands. The latter extend beyond the fault where the overall dilation is smaller. In the clay smear, the major principal stress is inclined by about

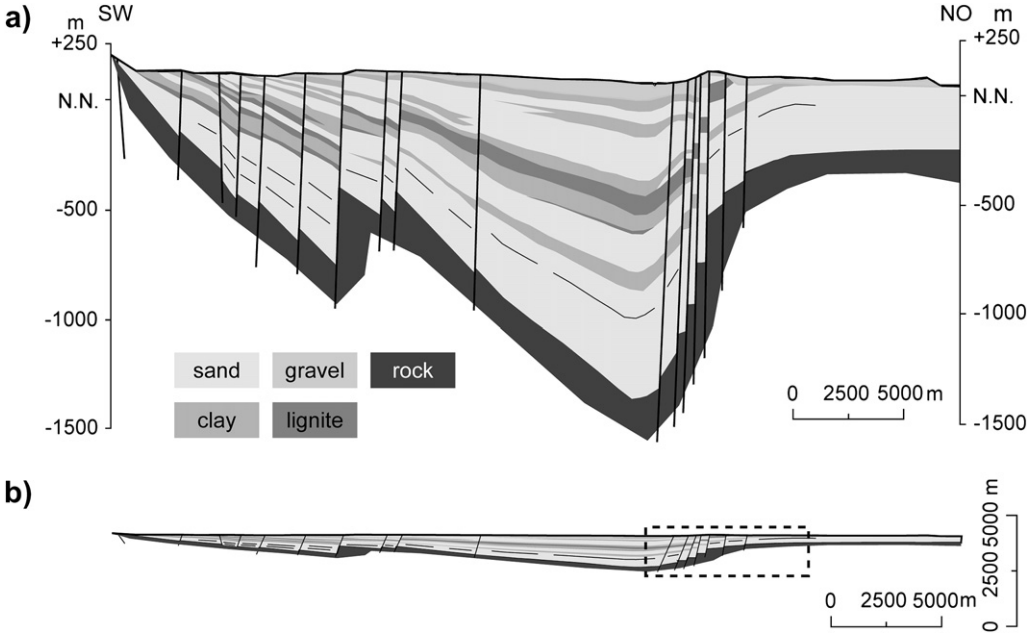

Fig. 7. Cross section of the Lower Rhenish Basin, simplified from Knufinke and Kothen (1995).

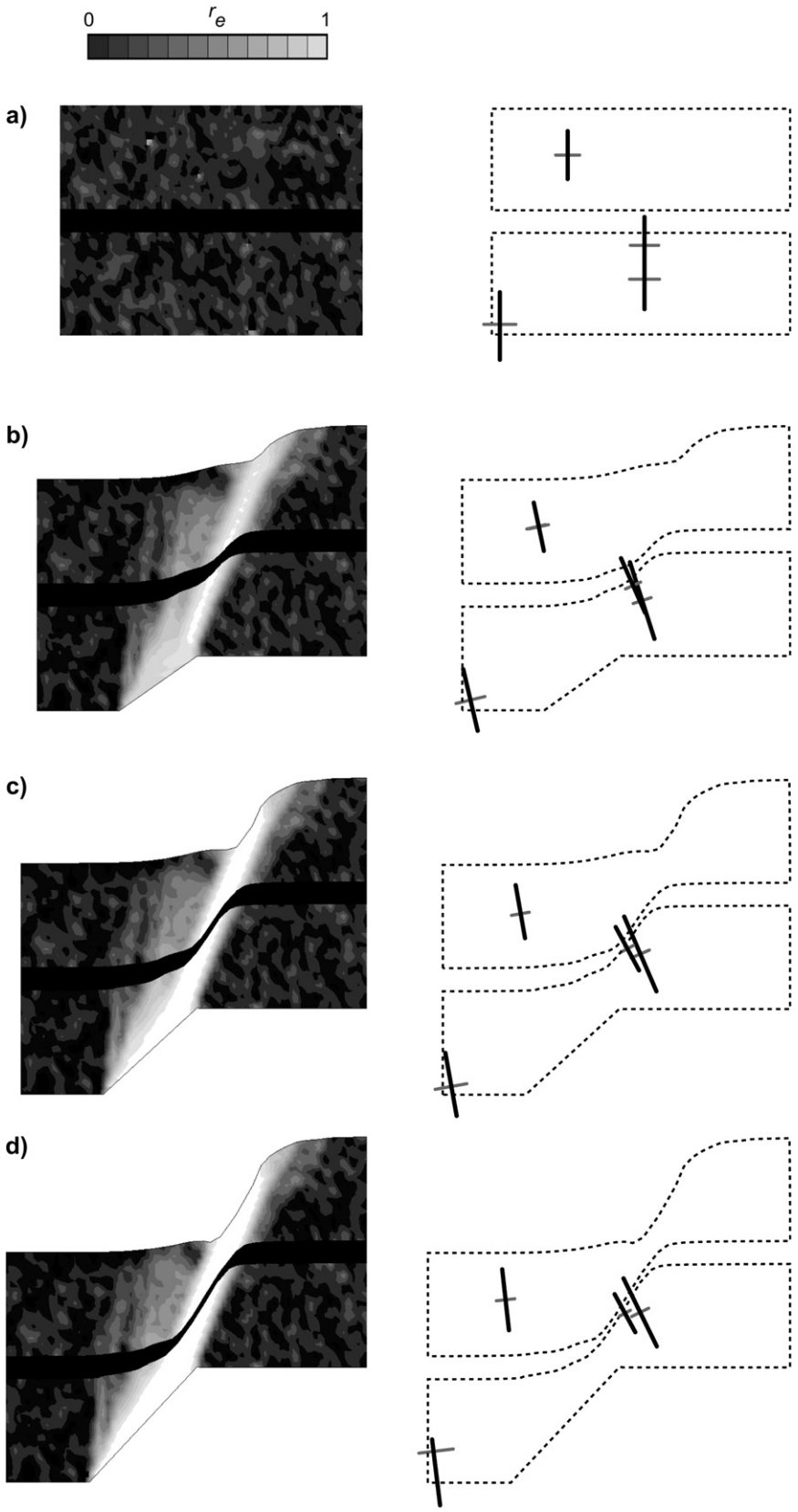

Fig. 8. Initial state (a) and simulated normal faulting with small (b), moderate (c) and bigger offset (d). Crosses indicate principal stresses.

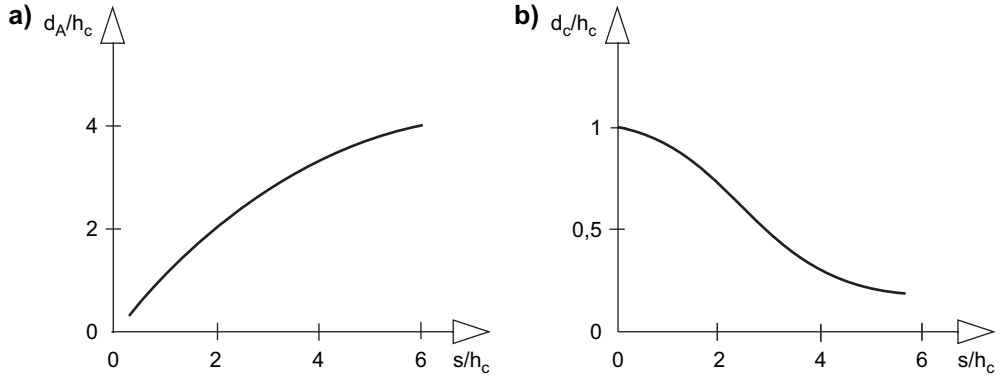

Fig. 9. Increase of fault width d_f (a) and decrease of clay smear thickness d_c (b) with offset s referred to clay layer height h_c, from the simulation of Fig. 8.

$45^\circ + \varphi_c/2$ against the fault normal. The adjacent sand has the same normal and shear stress along the contact, but a higher critical friction angle φ_c. The far-field stress remains nearly the one prior to the dislocation.

This mechanism is similar to the one proposed by Lehner and Pilaar (1995). They postulate a linearly viscous extrusion of clay from the source layer into the fault by a pressure gradient towards the same. They obtain the pressure gradient by assuming an isotropic far-field pressure; we calculate it with the lower stiffness and strength of peloids as against psammoids. The kinematics of Fig. 8 may be interpreted as a combination of extrusion and shearing. Our viscosity by Eq. (7) is strongly non-linear.

Our model produces some important features, which seem to be realistic. With increasing offset the clay smear thickness saturates at ca. 15% of the source layer thickness, whereas the fault gets wider and wider. Antithetic shear bands arise in the fault and in its vicinity. A detailed record of a fault with a clay smear provides a partial validation, Fig. 10. Pure shearing in the middle is clearly visible, and more antithetic shears on the dipping side than opposite of it. More details down to Riedels could be reproduced by local remeshing with polar quantities, cf. Figs. 4 and 5. The experience that clay smears work as sealings independent of the offset may serve as validation of the predicted asymptote in Fig. 9b.

6. Conclusions and outlook

Several features of normal faulting can be modelled by means of hypoplastic relations. These produce state limits as asymptotic states for monotonous deformations, ranging from isotropic compression via isochoric shearing to axial splitting or discing. Sand-like materials (psammoids) have a far higher solid hardness h_s and a higher critical friction angle φ_c than clay-like ones (peloids). The latter have a rate-dependent h_s, which corresponds to Norton's non-linear viscosity for stationary shearing and can cause creep or relaxation. Permanent particles are assumed, which may be justified for slow tectonic deformations. The few material parameters can be easily determined.

Peak states imply a reduction of deviator stress with further shearing, and localization to narrow bands where the material attains a stationary state (named critical). The band width is limited by the resistance against mutual grain rotations. With this polar extension, realistic patterns of normal shear bands in a small stretched psammoid rectangle are obtained down to bands of a few grains thickness. For bigger rectangles rather realistic primary shear band patterns and stress ratios can be obtained without polar terms. This holds also true with peloids if the stretching rate is slow enough so that the pore water pressure remains hydrostatic, which may be assumed for slow tectonic deformations.

Swarms of normal and antithetic faults can be obtained with initially homogeneous formations. For a psammoid layer with lower than critical relative void ratio, a free surface and stretching of the base between two smooth walls, a primary pattern of two swarms of normal faults and graben-type offsets at the outcrops are produced. This simulation and similar ones are confirmed by model tests, which can thus be substituted. For large *in situ* formations mesh sizes of a few grains are neither feasible nor necessary. This is demonstrated with an example of synsedimentary subsidence and stretching. Realistic swarms of normal and antithetic faults are obtained.

A normal fault with a clay smear is generated by dislocating a psammoid block with a thin peloid layer. With continued offset the clay smear thickness stabilizes at ca. 15% of the source layer thickness, whereas the fault gets wider. This mechanism is confirmed by field evidence and goes beyond the one proposed by Lehner and Pilaar (1995). It appears that other and more complex tectonic simulations could be carried out realistically with hypoplastic constitutive relations. 2D sand box tests can be simulated, up to details of shear bands with dilation, and more insight can be obtained than with measurements. For 3D cases and for typical *in situ* dimensions remeshing will be needed if shear bands of some grains thickness are to be grasped.

When relating the evolutions of state and shape hypoplastic simulations require a definition of initial state and boundary conditions. Hypoplastic state limits are of use to determine material parameters, and make the calculations robust with respect to inevitable uncertainties. State limits are attractors of the hypoplastic relations for representative volume elements. Similarly, shear patterns in the earth crust may be represented by *attractors in the large.*

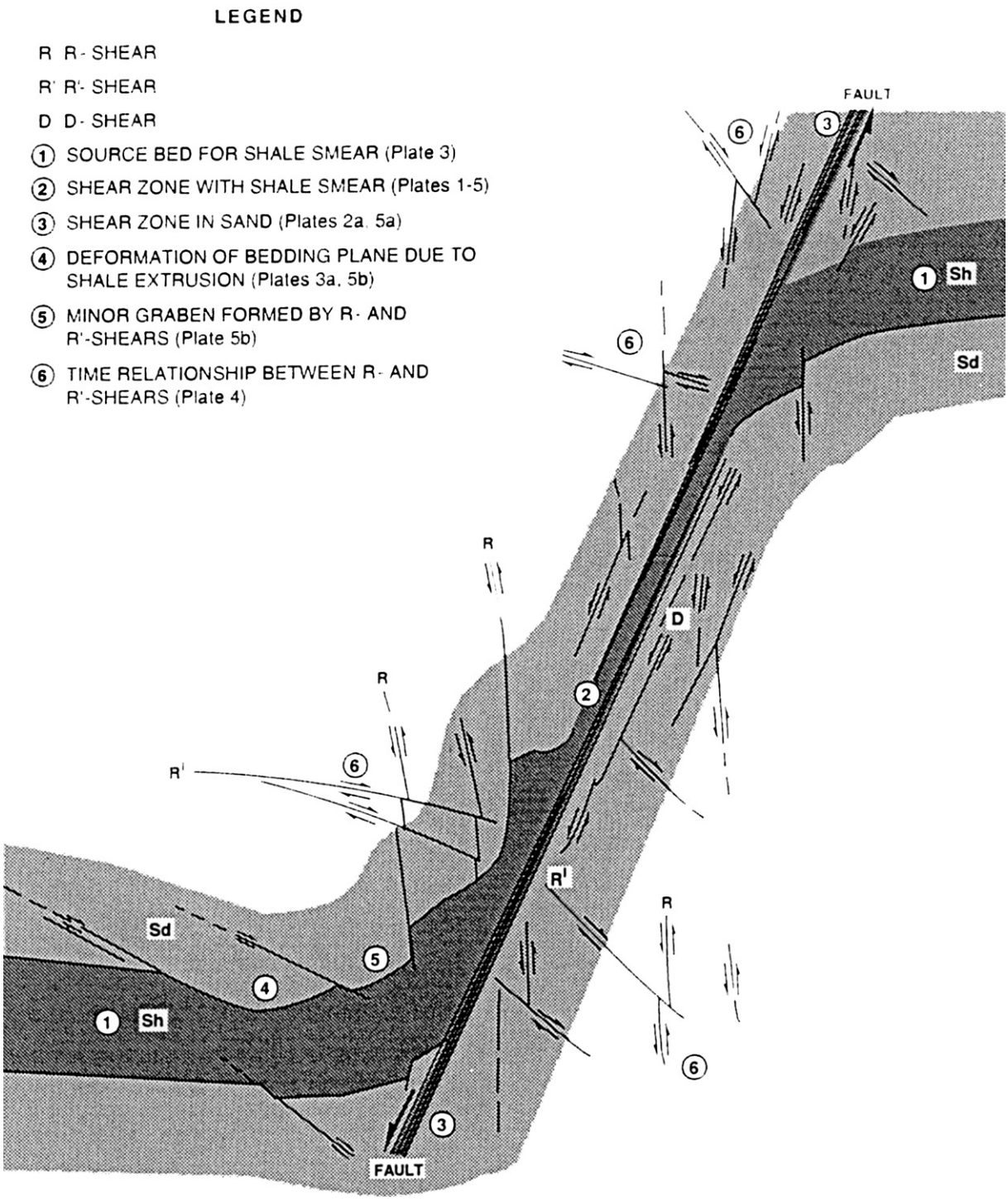

Fig. 10. A clay smear documented by Weber et al. (1978).

The *time scale* enters via filtration of pore water and via non-linear viscosity of peloids. For slow tectonic deformations hydrostatic pore water pressure p_w may be assumed, but creep and relaxation of peloids can produce substantial changes of shape and state. Other mechanisms can arise with non-hydrostatic p_w and related seepage forces. For instance, seismic shear waves can produce a temporary suspension or water film, so that layers are separated (Gudehus et al., 2004). A high p_w gradient across a clay smear can lead to an erosion breakthrough and a rise of mud in the fault. In all such cases hypoplastic simulations can be of use.

Acknowledgement

The present study is the result of cooperation with the RWE Power AG, in particular Prof. K. Pierschke, which is gratefully acknowledged.

References

Adachi, T., Oka, F., 1982. Constitutive equations for normally consolidated clay based on elasto-viscoplasticity. Soils and Foundations 22 (4), 57–70.

Bauer, E., 1996. Calibration of a comprehensive hypoplastic model for granular soils. Soils and Foundations, Jap. Geot. Soc. 38 (1), 1–12.

Desrues, J., 1998. Localisation patterns in ductile and brittle geomaterials. In: De Borst, Giessen (Eds.), Material Instabilities in Solids. Wiley, pp. 136–157.

Gudehus, G., 1996. A comprehensive constitutive equation for granular materials. Soils and Foundations 36 (1), 1–12.

Gudehus, G., Cudmani, R., Libreros-Bertini, A.B., Bühler, M.M., 2004. In-plane and anti-plane strong shaking of soil systems and structures. Soil Dynamics and Earthquake Engineering 24, 319–342.

Gudehus, G., Nübel, C., 2004. Evolution of shear bands in sand. Géotechnique 54 (3), 187–201.

Gudehus, G., 2006. Physical background of hypoplasticity. In: Wu (Ed.), Modern Trends in Geomechanics, 27.-29.06.05. Springer, Wien, pp. 17–37.

Karcher, C., 2003. Tagebaubedingte Deformationen im Lockergestein. Veröffentlichungen des Instituts für Bodenmechanik und Felsmechanik. Universität Karlsruhe. Heft 160.

Knufinke, H.V., Kothen, H., 1995. Die Tektonik der Niederrheinischen Bucht vor, während und nach der Hauptflächenbildung. Braunkohle, 473–479.

Lehner, F.K., Pilaar, W.F., 1995. The emplacement of clay smears in synsedimentary normal faults: inferences from field observations near Frechen, Germany. In: Møller Pederson, P., Koestler, A.G. (Eds.), Hydrocarbon Seals. Elsevier, pp. 39–50.

Mandl, G., 1988. Mechanics of Tectonics Faulting, Models and Basic Concepts. Elsevier, Amsterdam.

Niemunius, A., 2003. Extended hypoplastic models for soils. Monografia Nr. 34. Politechnika Gdansk, Gdansk.

Schoefield, A., Wroth, P., 1968. Critical State Soil Mechanics. McGraw Hill, London.

Schoefield, A., 2001. Re-appraisal of Terzaghi Soil Mechanics. In: Proc. Int. Conf. Geot. Engg. Balkema, vol. 4, p. 2473.

Tejchman, J., Gudehus, G., 2001. Shearing of a narrow granular layer with polar quantities. International Journal for Numerical and Analytical Methods in Geomechanics 25, 1–28.

Weber, K.J., Mandl, G. Pilaar, W.F., Lehner, F.K., Precious, R.G., 1978. The role of faults in hydrocarbon migration and trapping in Nigerian growth fault structures. Proceedings of 10th American Offshore Technology Conference, Houston, TX, vol. 4, pp. 2643–2653.

Wolf, H., König,., D., Triantafyllidis, Th., 2003. Examination of shear band formation in granular material. Journal of Structural Geology 25, 1229–1240.